CONDENSED MATTER PHYSICS

Nonreciprocal transport in gate-induced polar superconductor $SrTiO_3$

Yuki M. Itahashi[1], Toshiya Ideue[1]*, Yu Saito[1,2], Sunao Shimizu[3,4], Takumi Ouchi[5], Tsutomu Nojima[5], Yoshihiro Iwasa[1,3]*

Polar conductors/superconductors with Rashba-type spin-orbit interaction are potential material platforms for quantum transport and spintronic functionalities. One of their inherent properties is the nonreciprocal transport, where the rightward and leftward currents become inequivalent, reflecting spatial inversion/time-reversal symmetry breaking. Such a rectification effect originating from the polar symmetry has been recently observed at interfaces or bulk Rashba semiconductors, while its mechanism in a polar superconductor remains elusive. Here, we report the nonreciprocal transport in gate-induced two-dimensional superconductor $SrTiO_3$, which is a Rashba superconductor candidate. In addition to the gigantic enhancement of nonreciprocal signals in the superconducting fluctuation region, we found kink and sharp peak structures around critical temperatures, which reflect the crossover behavior from the paraconductivity origin to the vortex origin, based on a microscopic theory. The present result proves that the nonreciprocal transport is a powerful tool for investigating the interfacial/polar superconductors without inversion symmetry, where rich exotic features are theoretically prognosticated.

INTRODUCTION

Two-dimensional electron system (2DES) realized at the oxide surface or interface is a promising candidate for emergent physical properties and functionalities (*1*). Since it naturally hosts the spatial inversion symmetry breaking due to the structural asymmetry or crystal symmetry, characteristic spin-split bands with the spin-momentum locking emerge due to spin-orbit interaction (SOI), offering rich spintronic functionalities (*2*, *3*). Although 2DES is also an important platform for the exotic quantum phases such as quantum Hall effect (*4*) and superconductivity (*5*, *6*), the effect of the symmetry breaking on such quantum phases has been elusive.

One of the previously unidentified probes for broken inversion symmetry is the nonreciprocal electrical transport (*7*–*23*), which represents the directional dichroism of magnetoresistance and has been observed via DC measurement or AC lock-in technique (second harmonic resistance; see Materials and Methods) in several noncentrosymmetric crystals (*17*, *18*) or interfaces (*16*, *19*, *20*). In a polar semiconductor with Rashba-type SOI, the warped Fermi surface under in-plane magnetic field can cause the nonreciprocal transport (*18*). Recently, this experimental technique has been extended to the superconducting state, in which a large nonreciprocal response has been observed, while reports are limited in a few systems (*9*–*13*) and detailed mechanism has not been fully unveiled (*10*, *14*, *15*). According to the recent theoretical considerations (*14*, *15*), the nonreciprocal transport is an effective tool for probing the parity mixing of Cooper pairs (*24*, *25*) or vortex dynamics in noncentrosymmetric superconductors. Therefore, it is highly desired to examine the nonreciprocity around superconducting transition using a simple electron system with the broken inversion symmetry. The 2D superconductor with strong Rashba-type SOI can be a good candidate.

Here, we studied the nonreciprocal superconducting transport in a 2DES realized at the surface of $SrTiO_3$, which is an archetypal Rashba superconductor. We first observed a gigantic enhancement of the nonreciprocal response in the superconducting fluctuation region, which is six orders of magnitude larger than that in the normal state. With decreasing the temperature from the normal state to the superconducting fluctuation region, we found peculiar kink and sharp peak behavior in the nonreciprocal resistance, which can be understood in terms of crossover of nonreciprocal superconducting transport between the two distinct regions, i.e., nonreciprocal paraconductivity and the vortex-induced rectification effect. Our results unveil an unprecedented aspect of 2D polar superconductor, induced by vortex motion in noncentrosymmetric background around the Berezinskii-Kosterlitz-Thouless (BKT) transition.

RESULTS

To realize a 2D Rashba superconductor, we used an ion-gating technique on the surface of $SrTiO_3$. After fabricating Cr/Au electrodes on the atomically flat surface of $SrTiO_3$ (*26*, *27*), ionic liquid was placed on the top to form the electric double-layer transistor (EDLT) structure (Fig. 1A). Note that we did not use Ca-doped nor strained $SrTiO_3$ with a bulk ferroelectricity (*28*–*30*). We measured the first and second harmonic electric transport by a standard lock-in technique (see Materials and Methods).

First, we discuss the first harmonic resistance R^{ω}_{xx}, which corresponds to the linear resistance, near the superconducting transition for the gate voltage of V_G = 5.0 V. Figure 1B shows a temperature dependence of R^{ω}_{xx} at the low-current limit (I = 0.05 μA). Superconducting transition is observed at 0.31 K using the midpoint of the normal-state resistance, which can be regarded as the mean-field transition temperature T_{c0} (*31*). Black dashed line shows a fitting curve using the Halperin-Nelson formula $R^{\omega}_{xx} \sim R_N \exp\left(-2b\sqrt{\frac{T_{c0}-T}{T-T_{BKT}}}\right)$, where

[1]Quantum-Phase Electronics Center (QPEC) and Department of Applied Physics, The University of Tokyo, Tokyo 113-8656, Japan. [2]California NanoSystems Institute, University of California at Santa Barbara, Santa Barbara CA 93106, USA. [3]RIKEN Center for Emergent Matter Science (CEMS), Wako 351-0198, Japan. [4]Central Research Institute of Electric Power Industry (CRIEPI), Kanagawa 240-0196, Japan. [5]Institute for Materials Research, Tohoku University, Sendai 980-8577, Japan.
*Corresponding author. Email: ideue@ap.t.u-tokyo.ac.jp (T.I.); iwasa@ap.t.u-tokyo.ac.jp (Y.I.)

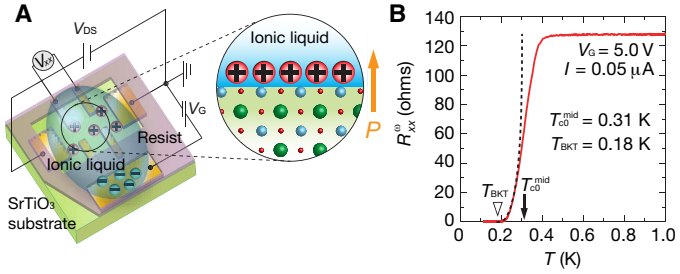

Fig. 1. Device image and gate-induced superconductivity in $SrTiO_3$. (**A**) Schematic image of $SrTiO_3$-EDLT. (**B**) Longitudinal first harmonic resistance R_{xx}^{ω} as a function of temperature T under zero magnetic field. The applied current was 0.05 μA, which can be regarded as low-current limit. Transition temperature defined by the midpoint of the resistive transition is estimated as T_{c0} = 0.31 K (black arrow). Black dashed line shows fitting curve by the Halperin-Nelson formula $R_{xx}^{\omega} \sim R_N \exp\left(-2b\sqrt{\frac{T_{c0}-T}{T-T_{BKT}}}\right)$, where R_N = 128 ohms is the normal-state resistance (T = 1.0 K), b = 1.17 is a dimensionless constant, and T_{BKT} = 0.18 K is BKT transition temperature (white triangle). The applied gate voltage V_G is 5.0 V at T = 260 K.

R_N = 128 ohms is the normal-state resistance (T = 1.0 K), b = 1.17 is a dimensionless constant, and T_{BKT} = 0.18 K is the BKT transition temperature. Because magnetic field is applied along in-plane direction in our experimental setup, we estimated the carrier density as $n \sim 2 \times 10^{14}$ cm^{-2} from the empirical relation between the carrier density and the normal-state resistance (*32*), instead of the Hall effect measurement. The value of n implies that the Fermi level locates far above the conduction band minimum and near the crossing point of d_{xy} and $d_{yz/zx}$ orbital band, where Rashba splitting is largely enhanced as discussed below (*32*–*36*).

Next, we focus on the second harmonic resistance, which represents the directional dichroism of the resistance. Figure 2 summarizes the first (R_{xx}^{ω}) and the second ($R_{xx}^{2\omega}$) harmonic magnetoresistance above and below T_{c0} for two kinds of in-plane B directions (red and blue lines represent the $I \perp B$ and $I \parallel B$ configurations, respectively). Figure 2 (A and B) shows R_{xx}^{ω} and $R_{xx}^{2\omega}$, respectively, for the normal states at T = 0.47 K and I = 20 μA, whereas Fig. 2 (C and D) shows R_{xx}^{ω} and $R_{xx}^{2\omega}$, respectively, for the superconducting fluctuation region at T = 0.22 K and I = 1 μA. In the normal state (above T_{c0}; Fig. 2, A and B), R_{xx}^{ω} shows slightly positive magnetoresistance, and $R_{xx}^{2\omega}$ is proportional to B. This B linear dependence of $R_{xx}^{2\omega}$ is consistent with the previous reports of nonreciprocal charge transport measurement for polar conductors (*16*, *18*, *23*). In the superconducting fluctuation region (below T_{c0}; Fig. 2, C and D), on the other hand, R_{xx}^{ω} exhibits a large positive magnetoresistance reflecting the B-driven superconductivity weakening, while $R_{xx}^{2\omega}$ shows sharp maximum and minimum at B = −0.1 and 0.1 T, respectively. Such an antisymmetric peak/valley structure of $R_{xx}^{2\omega}$ has been also observed in superconducting WS_2 nanotube (*9*) and gated MoS_2 (*10*, *12*). In Fig. 2 (B and D), finite $R_{xx}^{2\omega}$ can be observed only when B was applied perpendicularly to I, while it becomes negligibly small when B is parallel to I although there is little difference in R_{xx}^{ω} between two current directions. This direction-dependent $R_{xx}^{2\omega}$ indicates that nonreciprocal charge transport at the surface of $SrTiO_3$ can be attributed to the polar symmetry (*18*), both in the superconducting fluctuation region and the normal state.

To compare the magnitude of nonreciprocity between the normal state and superconducting fluctuation region, we calculated the γ defined by $\gamma = \frac{2R_{xx}^{2\omega}}{R_{xx}^{\omega}BI}$, which represents a coefficient of the nonreciprocal resistance (see Materials and Methods in detail). Figure 2E shows temperature dependence of γ for both the normal state (purple circles and dots) and the superconducting fluctuation region (orange circles and dots). Note that superconductivity is quenched even below T_{c0} under the large current (I = 20 μA). Thus, obtained γ below T_{c0} (purple dots) agrees well with the data at the normal-state data (purple symbols) in Fig. 2E. In the normal state, γ increases as temperature decreases and lastly reaches the value of γ ~10, which is of the same order of magnitude as that reported for $SrTiO_3$ (111) surface (*23*). The saturation behavior at low temperature is also consistent with the previous study of BiTeBr (*18*). In marked contrast, γ in the superconducting fluctuation region with I = 0.9 μA is largely enhanced as T decreases, becoming 10^6 times larger than that in the normal state. So far, nonreciprocal transport has been reported separately in the normal state (*18*–*23*) and superconducting fluctuation region (*9*–*12*) in any materials. The present result is the first simultaneous observation of the nonreciprocal responses, both in the normal and superconducting fluctuation region in an identical sample, clearly demonstrating the gigantic enhancement of γ in the superconducting fluctuation region.

We also measured the current I dependence of second harmonic signals in the normal state and superconducting fluctuation region. Figure 3A shows $R_{xx}^{2\omega}(B)$ at T = 0.85 K (normal state) under various I values. $R_{xx}^{2\omega}$ shows an almost linear B dependence for each current. In Fig. 3B, we plot the magnitude of $|R_{xx}^{2\omega}|$ at B = 3 T as a function of I. It increases lineally with I, indicating the second-order nonlinear voltage of the current. For the superconducting fluctuation region (T = 0.22 K; Fig. 3C), $R_{xx}^{2\omega}$ shows a peak structure as a function of B as discussed in Fig. 2D. Since the peak position depends on the current value, we focus on the low-field region where $R_{xx}^{2\omega}$ linearly increases with B. Current I dependence of $|R_{xx}^{2\omega}|$ at B = 0.1 T is shown in Fig. 3D. It first lineally increases with I, reaches the maximum around I = 1 μA, and is lastly suppressed, reflecting the suppression of the superconductivity by the high enough current. This behavior indicates that at the low-field and low-current region, the nonreciprocal response satisfies $R_{xx}^{2\omega} \propto BI$ also in the superconducting fluctuation region.

To further investigate the possible origin of nonreciprocal superconducting transport in the present system, we measured the temperature dependence of R_{xx}^{ω} and $R_{xx}^{2\omega}$ around the superconducting transition. Figure 4 (A and B) shows the magnetic field dependence of R_{xx}^{ω} (Fig. 4A) and $R_{xx}^{2\omega}$ (Fig. 4B) at various temperatures. In a wide temperature range, positive magnetoresistance (R_{xx}^{ω}) and peak structure of $R_{xx}^{2\omega}$ have been observed similarly to Fig. 2 (C and D). Note that with further increasing B, R^{ω} approaches R_N without exceeding it, as shown in fig. S3. In particular, $R_{xx}^{2\omega}$ is largely enhanced during the superconducting transition, which indicates that superconducting fluctuations in a 2D system remarkably affect the rectification effect. In 2D superconductors, it is well known that the resistive behavior around T_{c0} is governed by either amplitude or phase fluctuations of superconducting order parameter. For $T > T_{c0}$, the amplitude fluctuation (Aslamazov-Larkin type) causes the excess paraconductivity, while for $T_{BKT} < T < T_{c0}$, the phase fluctuation, which results in the motion of thermally excited vortex-antivortex pairs, plays a dominant role in the resistivity values.

To clarify the effect of these fluctuations on the first and second harmonic resistance, we scanned the temperature variation of R_{xx}^{ω} (Fig. 4C) and γ (Fig. 4D) at B = 0.05 T and I = 0.9 μA, where $R_{xx}^{2\omega}$ is proportional to both B and I. Since we applied the relatively large current in this measurement to probe the nonreciprocal transport clearly in

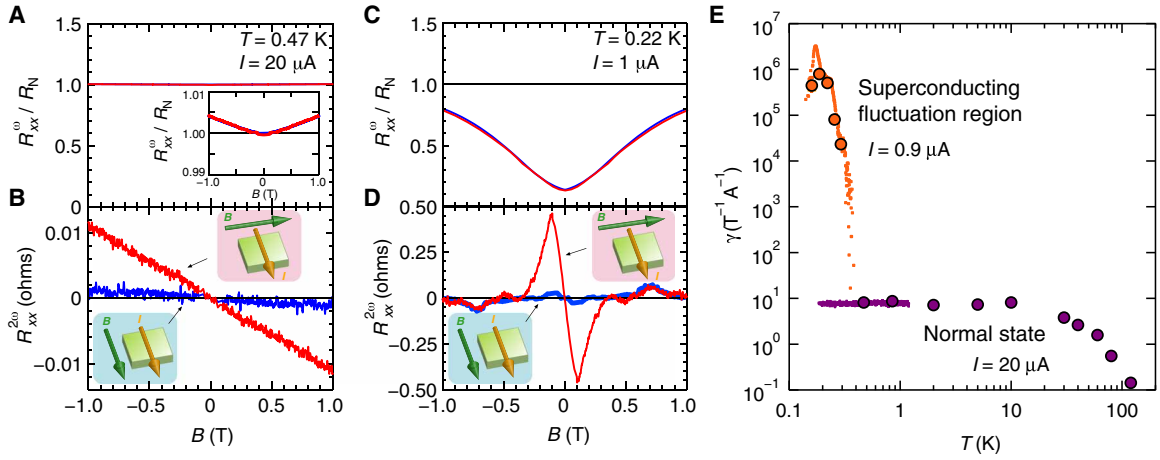

Fig. 2. Magnetotransport of gate-induced 2D $SrTiO_3$ for both the normal and superconducting states and enhancement of the nonreciprocal transport in the superconducting fluctuation region. (**A**) First and (**B**) second harmonic magnetoresistance (R^{ω}_{xx} and $R^{2\omega}_{xx}$, respectively) above T_{c0} (normal state, $T = 0.47$ K and $I = 20$ μA) as a function of in-plane magnetic field B perpendicular (red) or parallel (blue) to I. Insets in (A) and (B) show the magnified view of $R^{\omega}_{xx}(B)$ and schematics of the measurement configuration (directions of B and I), respectively. (**C**) R^{ω}_{xx} and (**D**) $R^{2\omega}_{xx}$ below T_{c0} (superconducting fluctuation region, $T = 0.22$ K and $I = 1$ μA) as a function of in-plane B perpendicular (red) or parallel (blue) to I. In (A) to (D), R^{ω}_{xx} is normalized by the normal-state resistance $R_N = 128$ ohms, and $R^{\omega}_{xx}/R^{2\omega}_{xx}$ is symmetrized/antisymmetrized as a function of B (see Materials and Methods). (**E**) Temperature dependence of $\gamma = \frac{2R^{2\omega}_{xx}}{R^{\omega}_{xx}BI}$ in the normal state ($I = 20$ μA) and superconducting fluctuation region ($I = 0.9$ μA). Purple (normal state) and orange (superconducting fluctuation region) circles were extracted from the measurement of magnetic field scan of $R^{2\omega}_{xx}$ at low B below 0.1 T, while purple (normal state) and orange (superconducting fluctuation region) dots were plotted from the temperature scan of $R^{2\omega}_{xx}$ under $B = 3$ and 0.05 T, respectively.

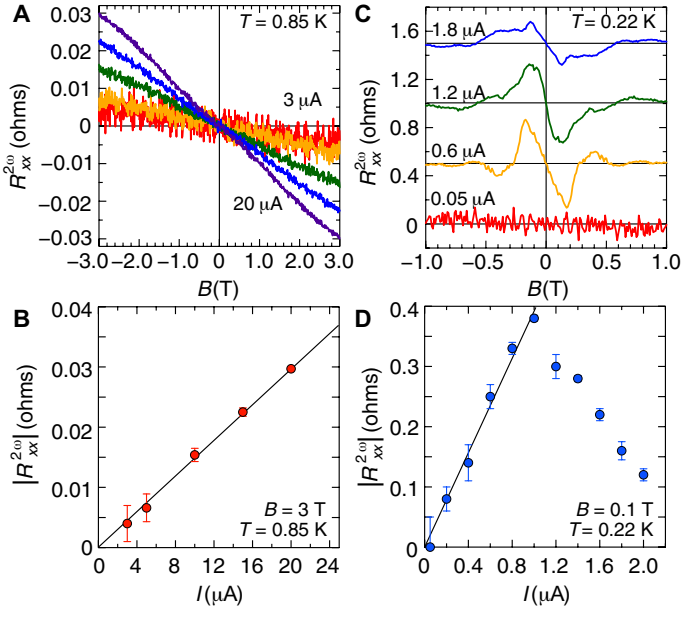

Fig. 3. Current dependence of the second harmonic magnetoresistance in the normal and the superconducting fluctuation region. (**A**) Second harmonic magnetoresistance $R^{2\omega}_{xx}$ at $T = 0.85$ K under $I = 3$ μA (red), 5 μA (orange), 10 μA (green), 15 μA (blue), and 20 μA (purple). $R^{2\omega}_{xx}$ is antisymmetrized as a function of B. (**B**) $|R^{2\omega}_{xx}|$ at $B = 3$ T as a function of I, which is extracted from (A). Black solid line shows linear fitting as a function of I. (**C**) Magnetic field dependence of $|R^{2\omega}_{xx}|$ at $T = 0.22$ K under $I = 0.05$ μA (red), 0.6 μA (orange), 1.2 μA (green), and 1.8 μA (blue). Each curve is shifted vertically by 0.5 ohms and antisymmetrized as a function of B. (**D**) Current dependence of $|R^{2\omega}_{xx}|$ at $B = 0.1$ T, where $R^{2\omega}_{xx}$ is regarded as a linear function of B. In low-current region ($I \leq 1$ μA), $|R^{2\omega}_{xx}|$ linearly increases (black solid line) with I.

all temperature range, R^{ω}_{xx} and γ are slightly different from those in the low-current limit. However, although relatively large current and in-plane magnetic field are applied, zero-resistance state is observed at the lowest temperature (Fig. 4C), implying the existence of the BKT transition. The characteristic structures appear in the temperature variation of γ (Fig. 4D), i.e., a kink structure around $T = 0.24$ K, followed by a prominent peak structure at $T = 0.17$ K.

DISCUSSION

In noncentrosymmetric 2D superconductors with in-plane magnetic field, two types of nonreciprocal charge transport are theoretically proposed (*14*, *15*): (i) nonreciprocal paraconductivity in the amplitude fluctuation region and (ii) vortex-induced rectification effect in the phase fluctuation region. The former mechanism predicts the enhancement of γ toward T_{c0} ($\gamma(T) = \gamma_s \left(1 - \frac{R(T)}{R_N}\right)^2$, where γ_s is γ at T_{c0} and $R_N = 128$ ohms is R^{ω}_{xx} at $T = 1.0$ K). The latter is expected to show the divergence of γ toward T_{c0} ($\gamma(T) \propto (T_{c0} - T)^{-1}$) and T_{BKT} ($\gamma(T) \propto (T - T_{BKT})^{-3/2}$). Below T_{BKT}, it is also predicted that both R^{ω}_{xx} and $R^{2\omega}_{xx}$ disappear.

It seems that the above scenario is consistent with observed characteristic structures in the temperature dependence of γ (Fig. 4D). Considering the correspondence between the present results and theory, we regard the kink and peak positions in Fig. 4D as the effective superconducting transition temperature (T^{eff}_{c0}) and BKT transition temperature (T^{eff}_{BKT}), respectively, under the finite current and magnetic field.

With decreasing temperature from the normal to the superconducting state, the nonreciprocal transport originating from the

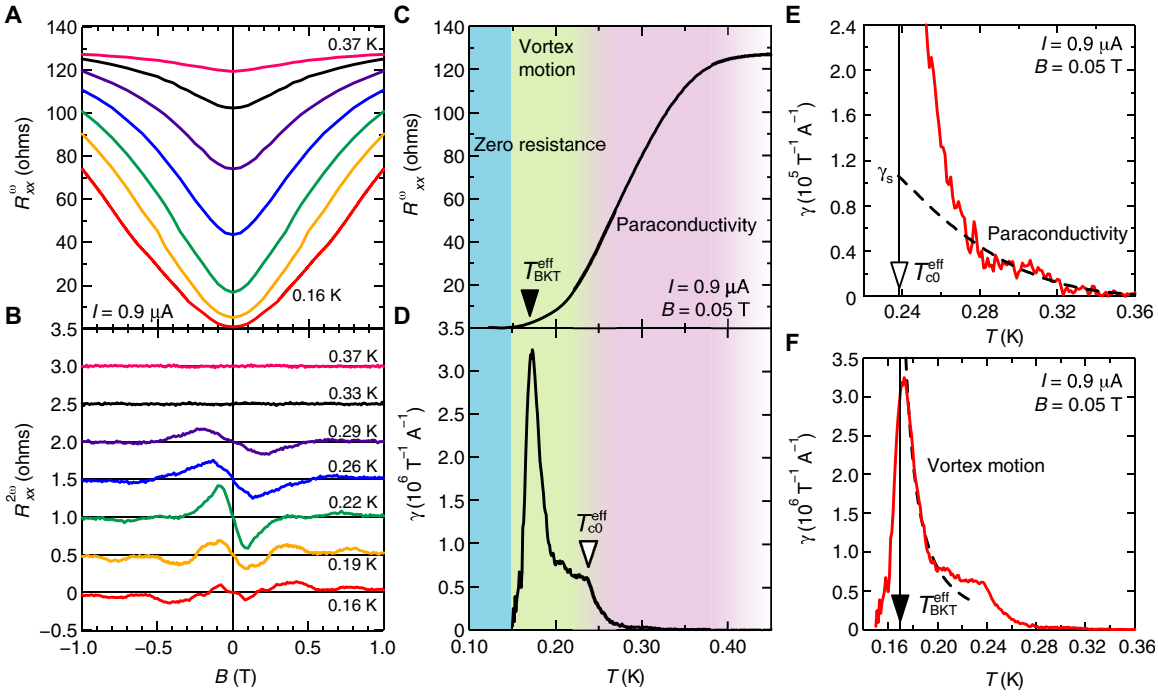

Fig. 4. Temperature dependence of the magnetoresistance and the nonreciprocal transport. Magnetic field dependence of (**A**) the first (R_{xx}^{ω}) and (**B**) the second ($R_{xx}^{2\omega}$) harmonic magnetoresistance at $T = 0.16$ K (red), 0.19 K (orange), 0.22 K (green), 0.26 K (blue), 0.29 K (purple), 0.33 K (black), and 0.37 K (pink), respectively. In (B), each curve is shifted vertically by 0.5 ohms. $R_{xx}^{\omega}/R_{xx}^{2\omega}$ is symmetrized/antisymmetrized as a function of B. Temperature variation of (**C**) R_{xx}^{ω} and (**D**) γ under $B = 0.05$ T and $I = 0.9$ μA. In this region, $R_{xx}^{2\omega}$ is linear as a function of B and I (Figs. 3D and 4B). R_{xx}^{ω}/γ is symmetrized/antisymmetrized as a function of B. Characteristic structure (kink structure around $T = 0.24$ K and peak structure around $T = 0.17$ K) appears in (D), according to which we can identify two regions of the nonreciprocal transport of different origins, i.e., paraconductivity region and vortex region. At the lowest temperature, zero-resistance state is observed, where R_{xx}^{ω} and γ becomes negligibly small. Magnification of γ in (**E**) paraconductivity region and (**F**) vortex region. Black dashed line in (E) shows fitting curve by $\gamma(T) = \gamma_s\left(1 - \frac{R(T)}{R_N}\right)^2$, and black dashed line in (F) indicates fitting curve by $\gamma(T) = C\left(T - T_{BKT}^{eff}\right)^{-3/2}$. Normal-state resistance $R_N = 128$ ohms is defined as R_{xx}^{ω} at $T = 1.0$ K.

amplitude fluctuation developed (*14*, *15*). Temperature dependence of γ far above T_{c0}^{eff} can be well fitted by $\gamma(T) = \gamma_s\left(1 - \frac{R(T)}{R_N}\right)^2$ with fitting parameter γ_s of 1.0×10^5 $T^{-1}A^{-1}$, as shown in Fig. 4E. The deviation below $T = 0.27$ K can be attributed to the evolution of the vortex-induced rectification effect as discussed below. According to the theory (*14*, *15*), emergence of the nonreciprocal paraconductivity in the Rashba superconductor manifests the parity mixing of the Cooper pairs. In the simplest Rashba system, γ_s is related with the ratio of the paring interactions $r_t = \frac{2V^u}{V^g + V^u}$ (V^g and V^u are an even and odd parity interaction, respectively). Estimated r_t is about 0.6 (see the Supplementary Materials), which is much larger than theoretically assumed value of $r_t \sim 0.1$ (*15*). To explain this discrepancy, we calculated the subband structure of electric field–induced 2DES at the surface of $SrTiO_3$ when $n = 2.0 \times 10^{14}$ cm^{-2} (see the Supplementary Materials in detail). A simple calculation revealed that the Fermi surface locates around the crossing point of d_{xy} and d_{yz} orbital bands, where the Rashba effect is largely enhanced (*36*). The observed large r_t might have captured this enhancement of Rashba-type SOI. Quantitative argument of γ_s in such a highly nonparabolic region and its relation to the parity mixing should be further studied in the future.

Last, we focus on γ for $T_{BKT}^{eff} < T < T_{c0}^{eff}$, where the phase fluctuation, that is, the motion of thermally excited vortices and antivortices, gives a dominant contribution. Reflecting direction-dependent Cooper-pair density originating from symmetry breaking under the magnetic field, free vortices/antivortices produce the nonreciprocal magnetoresistance in this low-temperature region (*15*). This mechanism of vortex-induced rectification effect predicts the divergence of γ toward T_{BKT} and T_{c0} with the relation of $\gamma(T) \propto (T - T_{BKT})^{-3/2}$ and $\gamma(T) \propto (T_{c0} - T)^{-1}$, respectively (*15*). We attribute the kink at T_{c0}^{eff} in Fig. 4D to the latter anomaly. The former should correspond to the peak structure at T_{BKT}^{eff}. Actually, temperature variation of γ is well described by $\gamma(T) = C\left(T - T_{BKT}^{eff}\right)^{-3/2}$ with a fitting parameter $C = 6200$ $T^{-1}A^{-1}$ $K^{3/2}$ (Fig. 4F). Note that below T_{BKT}^{eff}, non-ohmic resistance remains because large current dissociates vortex-antivortex pairs. However, γ rapidly decreases down to zero with decreasing temperature, and when R_{xx}^{ω} is zero, $R_{xx}^{2\omega}$ also becomes zero (see the Supplementary Materials), which is consistent with the theoretical consideration (*14*, *15*). Hence, the experimentally observed temperature dependence of γ in Fig. 4F agrees with the microscopic theoretical picture of free motion of thermally excited vortices and antivortices in polar 2D superconductors. This result proves that the nonreciprocal response is a powerful tool for the nature of noncentrosymmetric superconductors.

Another remarkable feature of the second harmonic magnetoresistance is the oscillating behavior as seen in Fig. 4B (for example, $T = 0.26$, 0.19, and 0.16 K) and even in the raw data (see the Supplementary Materials). It is well known that such an oscillating behavior

can appear in various physical quantities of superconductors such as magnetoresistance and Nernst effect due to the vortex matching effect, where the number of vortices matches the lattice constant or artificial structures (*37*–*40*). However, the detailed origin of the oscillating behavior in $R_{xx}^{2\omega}$ is the future problem.

We also note that in a recent study (*13*), the authors studied the nonreciprocal superconducting transport at Bi_2Te_3/FeTe, which has the similar interfacial symmetry breaking as the present system. They discussed the potential effect of the interplay between the topological surface state of Bi_2Te_3 and proximity-induced superconductivity. Although the electronic states and possible microscopic mechanisms are different in these two interfaces (the topological surface state at Bi_2Te_3/FeTe and Rashba effect at the $SrTiO_3$ surface), we believe that the nonreciprocal transport can universally appear at the interfacial superconductivity with polar symmetry, providing not only a previously unknown functionality of superconductivity but also important information of the electronic state and paring mechanism in noncentrosymmetric superconductors. The study of the nonreciprocal transport in other interfacial superconducting systems is an interesting and important future topic.

In summary, we studied the nonreciprocal transport in gate-induced 2D superconductor $SrTiO_3$. We successfully probed the marked jump of nonreciprocal transport from the normal to the superconducting states, providing a direct proof of the giant enhancement of the nonreciprocal transport in the superconducting fluctuation region. Moreover, the temperature dependence of γ is well explained by the recent microscopic theory, particularly in the phase fluctuation region. The amplitude fluctuation region, which might signal the parity mixture of the Cooper pairs, was left to be explained quantitatively, considering the complexity of the conduction band, such as multibands and strong nonparabolicity. In addition, doped $SrTiO_3$ shows the ferroelectricity (*28*–*30*), where bulk inversion symmetry is broken, and the relation between the nonreciprocal transport and the ferroelectric behavior should be further studied. The present results offer an important insight into polar superconductors, paving a new way of searching for the emergent properties and functionalities in the 2D oxide interfaces and superconductors.

MATERIALS AND METHODS

Device fabrication

A single crystal of $SrTiO_3$ was annealed at 1000°C for 3 hours to obtain an atomically flat (100) surface with a step-terrace structure (*26*). The surface termination is considered to be TiO_2 (*26*). After an Ar ion milling treatment, which makes the $SrTiO_3$ underneath the electrodes conductive (*27*), Au (90 nm)/Cr (5 nm) electrodes and a gate pad were patterned by a standard e-beam lithography process. After that, droplet of *N*,*N*-diethyl-*N*-(2-methoxyethyl)-*N*-methylammonium bis(trifluoromethylsulphonyl)imide (DEME-TFSI) was placed on the top to form the EDLT structure. Except for the channel and the gate electrode, the surface of the $SrTiO_3$ was covered by poly(methyl methacrylate) to avoid the contact of the ionic liquid.

Transport measurements

The first and second harmonic resistance was measured using AC lock-in amplifiers (Stanford Research Systems Model SR830 DSP) with a frequency of 13 Hz in a dilution refrigerator (see also below). The gate voltage was applied by a Keithley 2400 source meter at 260 K, which is above the glass transition temperature of DEME-TFSI, under high vacuum condition (less than 10^{-4} torr). Transport measurement was performed in a dilution refrigerator system (Triton, Oxford Instruments NanoScience) with a base temperature of 10 mK. Temperature was calibrated by Cernox and RuO_2 sensor.

As discussed in the previous works (*7*–*23*), the resistance of the noncentrosymmetric system can be written as

$$R = R^{(1)}(1 + \gamma BI)$$

where the first and second terms represent the linear resistance and nonreciprocal magnetoresistance, which is proportional to B and I, respectively. γ is a coefficient of nonreciprocal magnetoresistance. Output voltage then becomes

$$V = R^{(1)}(I + \gamma BI^2)$$

When the AC bias current with a frequency of ω ($I = I_0 \sin \omega t$) is applied, it leads to

$$\begin{aligned} V &= R^{(1)} I_0 \sin\omega t + R^{(1)} \gamma B I_0^2 \sin^2 \omega t \\ &= R^{(1)} I_0 \sin\omega t + \frac{1}{2}\gamma R^{(1)} B I_0^2 \left\{ 1 + \sin\left(2\omega t - \frac{\pi}{2}\right) \right\} \end{aligned}$$

Thus, by probing the first and the second harmonic resistance, we obtain

$$R^{\omega} \equiv \frac{V^{\omega}}{I_0} = R^{(1)}$$

and

$$R^{2\omega} \equiv \frac{V^{2\omega}}{I_0} = \frac{1}{2}\gamma R^{(1)} B I_0$$

The coefficient γ, which indicates the strength of the nonreciprocal transport, can be calculated by

$$\gamma = \frac{2R_{xx}^{2\omega}}{R_{xx}^{\omega} BI}$$

as described in Results and Discussion.

SUPPLEMENTARY MATERIALS

Supplementary material for this article is available at http://advances.sciencemag.org/cgi/content/full/6/13/eaay9120/DC1

Calculation of the subband structure and the Fermi energy

Symmetrization and antisymmetrization

Magnetoresistance under high magnetic field

γ in paraconductivity region and relation with the parity mixing

Nonreciprocal resistance at zero-resistance state

Fig. S1. Density of states and subband structures at the surface of $SrTiO_3$.

Fig. S2. Raw and antisymmetrized data of the second harmonic resistance.

Fig. S3. Temperature dependence of the magnetoresistance.

Fig. S4. The temperature variation of the second harmonic magnetoresistance.

REFERENCES AND NOTES

1. H. Y. Hwang, Y. Iwasa, M. Kawasaki, B. Keimer, N. Nagaosa, Y. Tokura, Emergent phenomena at oxide interfaces. *Nat. Mater.* **11**, 103–113 (2012).
2. E. Lesne, Y. Fu, S. Oyarzun, J. C. Rojas-Sánchez, D. C. Vaz, H. Naganuma, G. Sicoli, J.-P. Attané, M. Jamet, E. Jacquet, J.-M. George, A. Barthélémy, H. Jaffrès, A. Fert, M. Bibes, L. Vila, Highly efficient and tunable spin-to-charge conversion through Rashba coupling at oxide interfaces. *Nat. Mater.* **15**, 1261–1266 (2016).
3. R. Ohshima, Y. Ando, K. Matsuzaki, T. Susaki, M. Weiler, S. Klingler, H. Huebl, E. Shikoh, T. Shinjo, S. T. B. Goennenwein, M. Shiraishi, Strong evidence for d-electron spin transport at room temperature at a $LaAlO_3$/$SrTiO_3$ interface. *Nat. Mater.* **16**, 609–614 (2017).

4. Y. Matsubara, K. S. Takahashi, M. S. Bahramy, Y. Kozuka, D. Maryenko, J. Falson, A. Tsukazaki, Y. Tokura, M. Kawasaki, Observation of the quantum Hall effect in δ-doped $SrTiO_3$. *Nat. Commun.* **7**, 11631 (2016).
5. N. Reyren, S. Thiel, A. D. Caviglia, L. F. Kourkoutis, G. Hammerl, C. Richter, C. W. Schneider, T. Kopp, A.-S. Rüetschi, D. Jaccard, M. Gabay, D. A. Muller, J.-M. Triscone, J. Mannhart, Superconducting interfaces between insulating oxides. *Science* **317**, 1196–1199 (2007).
6. K. Ueno, S. Nakamura, H. Shimotani, A. Ohtomo, N. Kimura, T. Nojima, H. Aoki, Y. Iwasa, M. Kawasaki, Electric-field-induced superconductivity in an insulator. *Nat. Mater.* **7**, 855–858 (2008).
7. Y. Tokura, N. Nagaosa, Nonreciprocal responses from non-centrosymmetric quantum materials. *Nat. Commun.* **9**, 3740 (2018).
8. G. L. J. A. Rikken, J. Fölling, P. Wyder, Electrical magnetochiral anisotropy. *Phys. Rev. Lett.* **87**, 236602 (2001).
9. F. Qin, W. Shi, T. Ideue, M. Yoshida, A. Zak, R. Tenne, T. Kikitsu, D. Inoue, D. Hashizume, Y. Iwasa, Superconductivity in a chiral nanotube. *Nat. Commun.* **8**, 14465 (2017).
10. R. Wakatsuki, Y. Saito, S. Hoshino, Y. M. Itahashi, T. Ideue, M. Ezawa, Y. Iwasa, N. Nagaosa, Nonreciprocal charge transport in noncentrosymmetric superconductors. *Sci. Adv.* **3**, e1602390 (2017).
11. J. Lustikova, Y. Shiomi, N. Yokoi, N. Kabeya, N. Kimura, K. Ienaga, S. Kaneko, S. Okuma, S. Takahashi, E. Saitoh, Vortex rectenna powered by environmental fluctuations. *Nat. Commun.* **9**, 4922 (2018).
12. Y. M. Itahashi, Y. Saito, T. Ideue, T. Nojima, Y. Iwasa, Quantum and classical ratchet motions of vortices in a 2D trigonal superconductor. arXiv:1904.00611 [cond-mat. supr-con] (1 April 2019).
13. K. Yasuda, H. Yasuda, T. Liang, R. Yoshimi, A. Tsukazaki, K. S. Takahashi, N. Nagaosa, M. Kawasaki, Y. Tokura, Nonreciprocal charge transport at topological insulator/superconductor interface. *Nat. Commun.* **10**, 2734 (2019).
14. R. Wakatsuki, N. Nagaosa, Nonreciprocal current in noncentrosymmetric Rashba superconductors. *Phys. Rev. Lett.* **121**, 026601 (2018).
15. S. Hoshino, R. Wakatsuki, K. Hamamoto, N. Nagaosa, Nonreciprocal charge transport in two-dimensional noncentrosymmetric superconductors. *Phys. Rev. B* **98**, 054510 (2018).
16. G. L. J. A. Rikken, P. Wyder, Magnetoelectric anisotropy in diffusive transport. *Phys. Rev. Lett.* **94**, 016601 (2005).
17. F. Pop, P. Auban-senzier, E. Canadell, G. L. J. A. Rikken, N. Avarvari, Electrical magnetochiral anisotropy in a bulk chiral molecular conductor. *Nat. Commun.* **5**, 3757 (2014).
18. T. Ideue, K. Hamamoto, S. Koshikawa, M. Ezawa, S. Shimizu, Y. Kaneko, Y. Tokura, N. Nagaosa, Y. Iwasa, Bulk rectification effect in a polar semiconductor. *Nat. Phys.* **13**, 578–583 (2017).
19. K. Olejník, V. Novák, J. Wunderlich, T. Jungwirth, Electrical detection of magnetization reversal without auxiliary magnets. *Phys. Rev. B* **91**, 180402 (2015).
20. C. O. Avci, K. Garello, A. Ghosh, M. Gabureac, S. F. Alvarado, P. Gambardella, Unidirectional spin Hall magnetoresistance in ferromagnet/normal metal bilayers. *Nat. Phys.* **11**, 570–575 (2015).
21. K. Yasuda, A. Tsukazaki, R. Yoshimi, K. S. Takahashi, M. Kawasaki, Y. Tokura, Large unidirectional magnetoresistance in a magnetic topological insulator. *Phys. Rev. Lett.* **117**, 127202 (2016).
22. P. He, S. S.-L. Zhang, D. Zhu, Y. Liu, Y. Wang, J. Yu, G. Vignale, H. Yang, Bilinear magnetoelectric resistance as a probe of three-dimensional spin texture in topological surface states. *Nat. Phys.* **14**, 495–499 (2018).
23. P. He, S. McKeown Walker, S. S.-L. Zhang, F. Y. Bruno, M. S. Bahramy, J. M. Lee, R. Ramaswamy, K. Cai, O. Heinonen, G. Vignale, F. Baumberger, H. Yang, Observation of out-of-plane spin texture in a $SrTiO_3$(111) two-dimensional electron gas. *Phys. Rev. Lett.* **120**, 266802 (2018).
24. L. Fu, Parity-breaking phases of spin-orbit-coupled metals with gyrotropic, ferroelectric, and multipolar orders. *Phys. Rev. Lett.* **115**, 026401 (2015).
25. S. Kanasugi, Y. Yanase, Spin-orbit-coupled ferroelectric superconductivity. *Phys. Rev. B* **98**, 024521 (2018).
26. J. G. Connell, B. J. Isaac, G. B. Ekanayake, D. R. Strachan, S. S. A. Seo, Preparation of atomically flat $SrTiO_3$ surfaces using a deionized-water leaching and thermal annealing procedure. *Appl. Phys. Lett.* **101**, 251607 (2012).
27. D. W. Reagor, V. Y. Butko, Highly conductive nanolayers on strontium titanate produced by preferential ion-beam etching. *Nat. Mater.* **4**, 593–596 (2005).
28. C. W. Rischau, X. Lin, C. P. Grams, D. Finck, S. Harms, J. Engelmayer, T. Lorenz, Y. Gallais, B. Fauqué, J. Hemberger, K. Behnia, A ferroelectric quantum phase transition inside the superconducting dome of $Sr_{1-x}Ca_xTiO_{3-\delta}$. *Nat. Phys.* **13**, 643–648 (2017).
29. K. Ahadi, L. Galletti, Y. Li, S. Salmani-Rezaie, W. Wu, S. Stemmer, Enhancing superconductivity in $SrTiO_3$ films with strain. *Sci. Adv.* **5**, eaaw0120 (2019).
30. R. Russell, N. Ratcliff, K. Ahadi, L. Dong, S. Stemmer, J. W. Harter, Ferroelectric enhancement of superconductivity in compressively strained $SrTiO_3$ films. *Phys. Rev. Mater.* **3**, 091401 (2019).
31. Y. Saito, Y. Kasahara, J. Ye, Y. Iwasa, T. Nojima, Metallic ground state in an ion-gated two-dimensional superconductor. *Science* **350**, 409–413 (2015).
32. S. Shimizu, S. Ono, T. Hatano, Y. Iwasa, Y. Tokura, Enhanced cryogenic thermopower in $SrTiO_3$ by ionic gating. *Phys. Rev. B* **92**, 165304 (2015).
33. S. McKeown Walker, S. Riccò, F. Y. Bruno, A. de la Torre, A. Tamai, E. Golias, A. Varykhalov, D. Marchenko, M. Hoesch, M. S. Bahramy, P. D. C. King, J. Sánchez-Barriga, F. Baumberger, Absence of giant spin splitting in the two-dimensional electron liquid at the surface of $SrTiO_3$(001). *Phys. Rev. B* **93**, 245143 (2016).
34. P. D. C. King, S. McKeown Walker, A. Tamai, A. de la Torre, T. Eknapakul, P. Buaphet, S.-K. Mo, W. Meevasana, M. S. Bahramy, F. Baumberger, Quasiparticle dynamics and spin–orbital texture of the $SrTiO_3$ two-dimensional electron gas. *Nat. Commun.* **5**, 3414 (2014).
35. Z. Zhong, A. Tóth, K. Held, Theory of spin-orbit coupling at $LaAlO_3/SrTiO_3$ interfaces and $SrTiO_3$ surfaces. *Phys. Rev. B* **87**, 161102 (2013).
36. Y. Nakamura, Y. Yanase, Multi-orbital superconductivity in $SrTiO_3/LaAlO_3$ interface and $SrTiO_3$ surface. *J. Phys. Soc. Jpn.* **82**, 083705 (2013).
37. M. Nagao, S. Urayama, S. M. Kim, H. B. Wang, K. S. Yun, Y. Takano, T. Hatano, I. Iguchi, T. Yamashita, M. Tachiki, H. Maeda, M. Sato, Periodic oscillations of Josephson-vortex flow resistance in oxygen-deficient $YBa_2Cu_3O_x$. *Phys. Rev. B* **74**, 054502 (2006).
38. I. Swiecicki, C. Ulysse, T. Wolf, R. Bernard, N. Bergeal, J. Briatico, G. Faini, J. Lesueur, J. E. Villegas, Strong field-matching effects in superconducting $YBa_2Cu_3O_{7-\delta}$ films with vortex energy landscapes engineered via masked ion irradiation. *Phys. Rev. B* **85**, 224502 (2012).
39. M. N. Kunchur, C. L. Dean, B. I. Ivlev, Anomalous oscillatory magnetoresistance in superconductors. *Phys. Rev. B* **94**, 054504 (2016).
40. Y. Shiomi, J. Lustikova, E. Saitoh, Oscillatory Nernst effect in Pt|ferrite|cuprate-superconductor trilayer films. *Sci. Rep.* **7**, 5358 (2017).

Acknowledgments: We thank N. Nagaosa, S. Hoshino, R. Wakatsuki, and K. Hamamoto for discussions. **Funding:** Y.M.I. was supported by the Advanced Leading Graduate Course for Photon Science (ALPS). Y.S. was supported by the Japan Society for the Promotion of Science (JSPS) through a research fellowship for young scientists (Grant-in-Aid for JSPS Research Fellow, JSPS KAKENHI grant number JP15J07681). T.I. was supported by JSPS KAKENHI grant numbers JP19K21843, JP19H01819, and JP18H04216, JST PRESTO project (JPMJPR19L1) and grant from Yazaki Memorial Foundation for Science and Technology. This work was supported by JSPS KAKENHI grant numbers JP19H05602 and JP15H05884. **Author contributions:** Y.M.I., Y.S., T.I., and Y.I. conceived the research project. S.S. fabricated samples. Y.M.I. and Y.S. performed the experiments and analyzed the data with the help of S.S., T.O., and T.N. T.O. and T.N. performed subband calculations. Y.M.I., T.I., and Y.I. wrote the manuscript. All the authors led the physical discussions. **Competing interests:** The authors declare that they have no competing interests. **Data and materials availability:** All data needed to evaluate
the conclusions in the paper are present in the paper and/or the Supplementary Materials. Additional data related to this paper may be requested from the authors.

Submitted 29 July 2019
Accepted 3 January 2020
Published 27 March 2020
10.1126/sciadv.aay9120

Citation: Y. M. Itahashi, T. Ideue, Y. Saito, S. Shimizu, T. Ouchi, T. Nojima, Y. Iwasa, Nonreciprocal transport in gate-induced polar superconductor $SrTiO_3$. *Sci. Adv.* **6**, eaay9120 (2020).